The Astrophysical Journal, 717:348–356, 2010 July 1 doi:10.1088/0004-637X/717/1/348

A SUB-STELLAR COMPANION AROUND THE F7 V STAR HD 8673*

Michael Hartmann, Eike W. Guenther, and Artie P. Hatzes
Thüringer Landessternwarte Tautenburg, Sternwarte 5, D-07778 Tautenburg, Germany; michael@tls-tautenburg.de
Received 2009 October 16; accepted 2010 May 5; published 2010 June 11

ABSTRACT

In order to investigate the dependence of planet formation on stellar mass, we have been monitoring a sample of F-type main-sequence stars with the 2.0 m Alfred-Jensch telescope of the Thüringer Landessternwarte Tautenburg. This survey is based on high-precision radial velocity (RV) measurements using the coudé échelle spectrograph and an iodine absorption cell. We present RV measurements of the F7 V star HD 8673 that show a long-term variability of 1634 days with a semi-amplitude $K = 288\,\mathrm{m\,s^{-1}}$ that can be explained most reasonably by an orbiting sub-stellar companion with a minimum mass of 14.2 M_{Jup} in a high-eccentricity ($e = 0.723$) Keplerian orbit.

Key words: brown dwarfs – planetary systems – stars: individual (HD 8673) – stars: low-mass – techniques: radial velocities

1. INTRODUCTION

Precise measurements of the radial velocity (RV) of stars have led to the discovery of more than 400 extrasolar planets for more than a decade. Most surveys are focused on late-type solar-like stars (spectral type F8–K0) that cover only a small range in stellar mass (0.8–1.2 $M_{\odot}$). While some recent programs have also extended their planet searches to less massive M dwarfs (e.g., Bonfils et al. 2005; Butler et al. 2006; Endl et al. 2006) and more massive, evolved subgiants and giants (e.g., Hatzes et al. 2006; Johnson et al. 2006; Döllinger et al. 2007; Lovis & Mayor 2007; Niedzielski et al. 2007; Sato et al. 2007) as well as A-F type main-sequence (MS) stars (Galland et al. 2005; Guenther et al. 2009), our knowledge of how planet formation depends on stellar mass is still very limited. However, initial results show evidence that more massive stars tend to harbor more massive planets (Johnson et al. 2007a, 2007b; Lovis & Mayor 2007).

Theoretical models by Kennedy & Kenyon (2008) give a linearly rising probability with stellar mass from 0.4 to 3 $M_{\odot}$ that a given star hosts at least one gas giant planet. Considering a normalization to 6% for solar-mass stars, they predict that the frequency of having at least one giant planet is about 1% (10%) for 0.4 $M_{\odot}$ (1.5 $M_{\odot}$) stars. On the other hand, calculations by Kornet et al. (2006) show a different result. They conclude that the percentage of stars with massive planets decreases with increasing stellar mass at least from 0.5 to 4 $M_{\odot}$.

Since it is not yet possible to draw meaningful conclusions about the frequency and properties of exoplanets and their dependence on stellar mass because of the limited number of such objects around lower and higher mass stars, it is of primary importance to find more planetary companions around those stars in order to test theoretical models.

Therefore, we have started an RV survey to search for extrasolar planets and brown dwarfs around F-type MS stars with the 2.0 m Alfred-Jensch telescope at the Thüringer Landessternwarte (TLS) Tautenburg. Although the masses of F-stars range only between 1.1 and 1.7 $M_{\odot}$, an F-star survey may allow one to get a first glimpse of how the frequency and mass of planets depend on the mass of the host stars.

In this paper, we report the detection of a massive planetary or brown dwarf companion to the F7 V star HD 8673. In Section 2, we give the stellar properties of the host star. The observations are described in Section 3. A description of the RV determination as well as the orbital solution for the companion is given in Section 4. In Section 5, we investigate the nature of the observed RV variations. We conclude in Section 6 and give a summary of our results.

2. STELLAR PROPERTIES OF HD 8673

HD 8673 (HIP 6702, HR 410) is classified as F7 V star in the SIMBAD database and has a visual magnitude $V = 6.34$ and a color $B-V = 0.500 \pm 0.004$ (*Hipparcos* Catalog; ESA 1997; Perryman et al. 1997). Given the *Hipparcos* parallax $\pi = 26.14 \pm 0.79$ mas, the star is located at a distance of 38.3 ± 1.2 pc. Nordström et al. (2004) give a stellar mass of $1.28^{+0.05}_{-0.04}\,M_{\odot}$ and an age of 2.5 ± 0.4 Gyr, whereas Valenti & Fischer (2005) derive a mass of $1.36 \pm 0.20\,M_{\odot}$ and an age of $1.5^{+0.6}_{-0.9}$ Gyr. Studies by Takeda et al. (2007) yield values of $1.312^{+0.024}_{-0.020}\,M_{\odot}$ and 2.52 ± 0.24 Gyr, respectively. Furthermore, Ibukiyama & Arimoto (2002) achieve a higher value of 4.06 Gyr for the age. A more recent mass determination of 1.39 $M_{\odot}$ for this star is published by Fuhrmann (2008). A metallicity [Fe/H] of +0.16, −0.12, −0.01, +0.15, and +0.13 is given by Cayrel de Strobel et al. (2001), Ibukiyama & Arimoto (2002), Nordström et al. (2004), Valenti & Fischer (2005), and Fuhrmann (2008), respectively. These and further stellar parameters taken from the literature are summarized in Table 1.

3. OBSERVATIONS

HD 8673 belongs to a sample of F-type MS stars monitored as part of the Tautenburg Observatory Planet Search program (TOPS). Since 2002 July, a total of 135 spectra have been taken using the 2.0 m Alfred-Jensch telescope of the TLS and its coudé échelle spectrograph with resolving power $R = \lambda/\Delta\lambda = 67{,}000$. The spectra cover a wavelength range of 4700–7400 Å. The typical exposure time was 10–15 minutes yielding an average signal-to-noise ratio (S/N) of 65 per pixel at ∼4950 Å. During the observations, an iodine absorption cell was placed in the optical light path in front of the spectrograph's slit. Consequently, the resulting iodine absorption spectrum was then superposed on top of the current stellar spectrum providing

* Based on observations obtained at the 2.0-m Alfred-Jensch telescope at the Thüringer Landessternwarte Tautenburg.

Table 1
Stellar Properties of HD 8673

Parameter	Values
Spectral type	F7 V
$v \sin i$ (km s^{-1})	30[d], 26.9[e], 28.2 ± 1.0[g], 28.4 ± 0.8[h]
V (mag)	6.34[a], 6.310[d]
$B-V$ (mag)	0.500 ± 0.004[a]
M_V (mag)	3.39[d]
π (mas)	26.14 ± 0.79[a]
Distance (pc)	38.3 ± 1.2
[Fe/H] (dex)	+0.16[b], −0.12[c], −0.01[d], +0.15[e], +0.13[g]
$T_{\rm eff}$ (K)	6380[b], 6310[d], 6340[e], 6413[g]
log g (cgs)	4.50[b], 4.21[e], 4.19 ± 0.03[f], 4.21[g]
$M_\star$ ($M_\odot$)	$1.28^{+0.05}_{-0.04}$[d], 1.36 ± 0.20[e], $1.312^{+0.024}_{-0.020}$[f], 1.39[g]
$R_\star$ ($R_\odot$)	1.521 ± 0.049[e], 1.54 ± 0.06[f]
Age (Gyr)	4.06[c], 2.5 ± 0.4[d], $1.5^{+0.6}_{-0.9}$[e], 2.52 ± 0.24[f]

References. (a) ESA 1997; Perryman et al. 1997; (b) Cayrel de Strobel et al. 2001; (c) Ibukiyama & Arimoto 2002; (d) Nordström et al. 2004; (e) Valenti & Fischer 2005; (f) Takeda et al. 2007; (g) Fuhrmann 2008; (h) this paper.

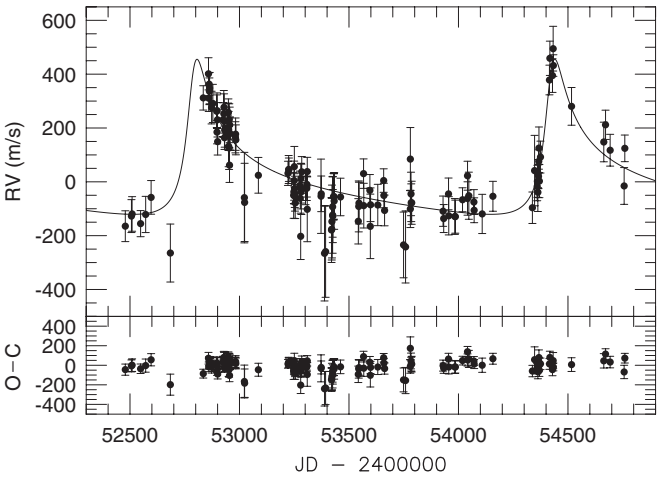

Figure 1. RV measurements of HD 8673 and best-fit Keplerian orbital solution (solid line). The RV residuals after subtracting the orbital solution are shown below.

a stable wavelength reference against which the stellar RV can be measured very precisely. Furthermore, it also allows us to determine the point spread function (PSF).

4. RADIAL VELOCITY MEASUREMENTS AND ORBITAL SOLUTION

In the first step, the standard CCD data reductions (bias-subtraction, flat-fielding, and spectral order extraction) were performed using IRAF[1] routines.

In the second step, the RVs were calculated by modeling the observed spectra with a high-S/N template of the star (without iodine cell) and a scan of our iodine cell taken at very high resolution with the Fourier Transform Spectrometer (FTS) of the McMath–Pierce telescope at Kitt Peak. The latter enabled us to compute the relative velocity shift between stellar and iodine absorption lines as well as to model the temporal and spatial variations of the instrumental profile (IP). See Valenti et al. (1995) and Butler et al. (1996) for a description of the principles behind this technique.

Each spectrum was typically split up into 130 small spectral segments (chunks) of ≈8–9 Å, where the RV was determined for each chunk individually. The errors were estimated from the scatter of the values determined for each chunk. The large $v \sin i$ of HD 8673 of 28.4 ± 0.8 km s^{-1} (see Table 1) and the relatively early spectral type boost the error to a mean (median) value of 71 m s^{-1} (62 m s^{-1}). Since we achieve an accuracy of 5 m s^{-1} for a star with a $v \sin i$ of 2 km s^{-1}, and since the errors of RV measurements are proportional to $v \sin i$, errors of about 60–70 m s^{-1} for HD 8673 are fully consistent with our expectations. Table 2 gives the RV measurements obtained for HD 8673. The corresponding time series is shown in Figure 1. It is obvious that the RV variations are non-sinusoidal but rather consistent with an orbiting highly eccentric body.

Since classical period search programs have difficulties in finding eccentric orbits, we used a novel approach for fitting the data. First, a Lomb–Scargle periodogram (Lomb 1976; Scargle 1982) was used to get an estimate of the RV period. The resulting power spectrum, which shows a strong peak at a period of about 1644 days, is displayed in Figure 2. Our program then phase-folded the data with all possible periods within a given interval. For each period, the best Keplerian orbit was determined by varying the eccentricity e and time of periastron T_0 until the χ^2 of the residual RV values about the current orbital solution was minimized. Here, it was not necessary to step also through the amplitude K, periastron angle ω, and RV offset RV$_0$ if some substitutions were applied (see Zechmeister & Kürster 2009). The best solution for all periods was then found as the maximum of $(\chi^2)^{-1}$. Tests showed that this algorithm is also able to find orbits with eccentricities larger than 0.4, which are more difficult to find with other methods. Figure 3 shows $(\chi^2)^{-1}$ of the RV residuals around Keplerian orbits of different periods between 625 and 2500 days. The χ^2 is minimal, i.e., $(\chi^2)^{-1}$ is maximal for a period of 1634 days. These orbital parameters were used as starting values for the nonlinear least-squares fitting program *GaussFit* (Jefferys et al. 1988). The orbital solution, including the uncertainties determined by *GaussFit* from a maximum likelihood estimation, is given in Table 3 and also shown as solid line in Figure 1. The parameters are fully consistent with the ones derived from the Keplerian periodogram. Using the calculated mass function $f(m) = (1.33 \pm 0.25) \times 10^{-6}\, M_\odot$ and the stellar mass of $1.36 \pm 0.20\, M_\odot$ (from Valenti & Fischer 2005) results in a minimum companion mass of $14.2 \pm 1.6\, M_{\rm Jup}$ and a semi-major axis $a = 3.02 \pm 0.15$ AU (Table 3).

To measure the quality of the fit, we computed the Keplerian periodogram power as defined by Cumming et al. (2008):

$$z_{\rm Kep}(\omega) = \frac{N-5}{4} \frac{\chi^2_{\rm const} - \chi^2_{\rm Kep}(\omega)}{\chi^2_{\rm Kep}(\omega_0)}, \quad (1)$$

which yielded $z_{\rm Kep} \approx 263$. The significance of the power was determined by assessing the probability that this power would arise purely due to noise. For a single-frequency search, the probability that a periodogram power exceeds a given value z_0 can be expressed analytically for Gaussian noise (Cumming et al. 2008):

$$\mathrm{Prob}(z > z_0) = \left(1 + \frac{N-3}{2} \frac{4z_0}{N-5}\right) \left(1 + \frac{4z_0}{N-5}\right)^{-\frac{N-3}{2}}. \quad (2)$$

The false alarm probability (FAP) for a search in a frequency

[1] IRAF is distributed by the National Optical Astronomy Observatory, which is operated by the Association of Universities for Research in Astronomy, Inc., under cooperative agreement with the National Science Foundation.

Table 2
Relative Radial Velocities for HD 8673

BJD (2,400,000+)	RV (m s^{-1})	σ (m s^{-1})
52,478.576207	−164.8	57.3
52,506.592152	−127.3	61.1
52,509.548364	−119.3	64.2
52,548.417515	−155.4	48.5
52,571.553059	−121.2	67.3
52,596.400315	−57.8	62.5
52,684.304319	−264.6	107.7
52,834.496922	311.8	45.2
52,858.484266	401.3	59.7
52,859.569292	310.8	49.3
52,861.570126	362.6	42.6
52,862.564715	336.4	49.6
52,863.579421	348.1	58.3
52,872.527998	275.8	60.7
52,878.457926	291.2	71.0
52,896.345813	262.1	60.8
52,897.428146	264.8	65.5
52,897.436329	184.7	43.6
52,899.275857	230.5	63.9
52,900.272580	149.3	49.7
52,925.272285	231.1	62.7
52,928.346926	253.0	86.3
52,929.441249	276.9	50.0
52,930.422501	224.6	43.5
52,931.381367	163.7	43.3
52,932.297141	192.3	63.5
52,947.336793	191.4	56.2
52,948.271051	225.8	66.7
52,949.372052	257.5	50.6
52,949.378059	174.8	58.5
52,950.396027	194.5	67.1
52,950.407450	132.1	76.0
52,952.364611	125.7	79.7
52,953.309416	231.2	58.6
52,954.414413	61.8	64.1
52,955.386113	211.5	66.0
52,956.369293	179.6	61.7
52,981.310401	165.4	57.8
52,982.271961	177.1	60.1
52,983.394285	155.9	55.6
53,022.227522	−58.7	168.1
53,023.339445	−76.5	145.3
53,086.262870	24.3	66.4
53,221.489786	31.5	44.9
53,224.524046	45.8	51.9
53,225.531727	45.0	43.5
53,247.341200	−50.3	85.2
53,248.455519	−37.1	44.4
53,249.542960	4.4	72.6
53,250.441485	56.3	75.1
53,251.460956	−25.8	56.0
53,252.487035	−52.7	42.4
53,253.426927	−44.0	64.9
53,254.442853	−78.4	58.1
53,275.504996	−13.4	53.3
53,277.535855	−61.4	39.2
53,279.402814	−202.6	86.1
53,280.502311	12.6	56.3
53,281.573737	−37.5	41.4
53,282.486731	−27.9	93.5
53,284.337288	37.2	56.6
53,301.388523	−23.6	61.4
53,307.512779	−9.4	47.1
53,307.526124	−24.0	45.3
53,309.420844	−102.1	120.4

Table 2
(Continued)

BJD (2,400,000+)	RV (m s^{-1})	σ (m s^{-1})
53,309.429606	37.9	53.0
53,372.340993	−53.6	138.0
53,373.247385	−44.6	66.2
53,388.321899	−265.8	176.8
53,393.250843	−259.4	169.6
53,420.274277	−179.0	120.7
53,421.276659	−175.9	114.5
53,422.269287	−147.4	135.3
53,425.305121	−123.6	141.8
53,425.317041	−92.8	112.9
53,426.250024	−127.2	98.6
53,429.310727	−55.2	87.1
53,431.278856	−54.5	84.4
53,432.287047	−71.2	105.2
53,461.280530	−56.3	69.7
53,542.548909	−146.7	84.2
53,544.534718	−91.3	94.6
53,545.545050	−78.9	77.4
53,566.563804	30.4	54.7
53,567.517094	−88.5	83.0
53,595.468553	−31.6	58.7
53,597.477277	−165.5	119.8
53,598.513302	−85.2	62.6
53,631.447497	−86.1	76.8
53,658.349633	4.7	43.6
53,659.371941	−50.8	45.6
53,662.521694	−106.3	57.1
53,749.229630	−234.5	122.1
53,758.352946	−241.9	134.0
53,780.286275	84.4	117.3
53,780.324513	−100.6	69.2
53,783.251798	−45.1	80.8
53,784.269595	−77.6	70.1
53,786.328475	−77.8	80.0
53,929.546801	−109.1	56.3
53,932.554044	−136.4	52.0
53,954.579514	−44.9	59.0
53,955.601652	−126.2	71.0
53,983.601669	−128.7	66.6
53,985.568887	−129.4	61.4
54,018.443043	−66.6	44.5
54,041.315282	−61.9	62.0
54,041.330340	22.7	53.8
54,047.295329	−51.6	87.5
54,070.373666	−75.1	46.1
54,071.529448	−105.7	46.2
54,108.326098	−119.3	72.9
54,157.262626	−53.7	55.6
54,337.533855	−96.3	58.5
54,347.538446	41.8	130.8
54,359.506220	−17.0	53.3
54,360.504530	2.0	59.6
54,362.493783	−38.7	71.4
54,363.512125	30.5	52.4
54,365.500561	20.1	45.5
54,366.489175	76.2	42.7
54,367.471434	125.4	78.4
54,369.482928	2.6	61.5
54,374.469445	92.0	59.2
54,415.356024	378.3	55.1
54,417.373460	459.0	63.7
54,429.316553	394.8	62.5
54,432.331422	494.7	83.1
54,433.299244	432.0	40.1
54,516.269484	280.4	70.1

Table 2
(Continued)

BJD (2,400,000+)	RV (m s^{-1})	σ (m s^{-1})
54,663.555323	148.0	73.6
54,671.575493	211.9	54.4
54,692.586664	117.4	59.0
54,756.510082	−15.4	68.4
54,759.518911	124.4	49.4

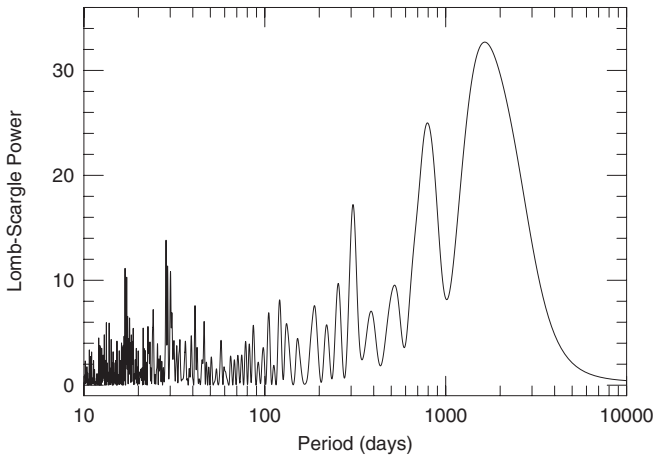

Figure 2. Lomb–Scargle periodogram of the RV data of HD 8673. The highest peak is visible at a period of 1644 days.

range is then given by

$$\mathrm{FAP} = 1 - [1 - \mathrm{Prob}(z > z_0)]^M \quad (3)$$

$$\approx M\ \mathrm{Prob}(z > z_0) \quad (F \ll 1), \quad (4)$$

where M is the number of independent frequencies, which can be simply estimated by $M \approx T\Delta f$, with $\Delta f = f_2 - f_1$ being the frequency range searched and T the duration of the data set. If $f_2 \gg f_1$, one can write $M \approx T f_2$ (Cumming 2004). On the other hand, Cumming (2004) discussed the effect of the uneven sampling on the number of independent frequencies and stated that $M \gg N$, in general by a factor of f_2/f_{Ny}, where $f_{\mathrm{Ny}} = N/(2\,T)$ is the Nyquist frequency. When searching for periods as short as 1 day, this leads to $M \approx 2\,T\,f_2 = 2\,T$ day^{-1}. Using these equations, one can calculate the FAP to be $\approx 10^{-57}$.

In order to search for any additional signals in the RV data, we analyzed the RV residuals. Figure 4 shows the corresponding Lomb–Scargle periodogram. The highest peak is visible at a period of about 120 days having a power of 9.58. The significance of this signal was estimated using a bootstrap randomization technique (Kürster et al. 1997). The RV residual values were randomly shuffled, keeping the observing times fixed, and a periodogram was then computed. The fraction of random periodograms having power higher than the periodogram of the real data gave an estimate of the FAP that the detected signal would originate from noise. After 10,000 "shuffles," we derived an FAP of 9%. We thus consider this period to be not yet significant. Nevertheless, it is worth to continue monitoring this star as a possible additional planetary companion would make this system very interesting.

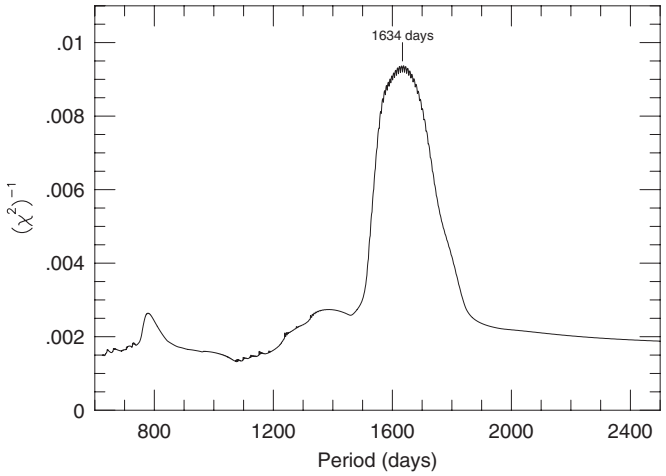

Figure 3. $(\chi^2)^{-1}$ of the data points around Keplerian orbits of different periods. χ^2 is minimal for a period of 1634 days.

Table 3
Orbital Elements of the Companion of HD 8673

Parameter	Value
P (days)	1634 ± 17
T_0 (BJD)	$2\,454\,420.5 \pm 7.9$
K (m s^{-1})	288 ± 16
e	0.723 ± 0.016
ω (deg)	323.4 ± 3.5
$\sigma(O-C)$ (m s^{-1})	71
$a_1 \sin i$ (10^{-3} AU)	29.9 ± 1.9
$f(m)$ ($M_\odot$)	$(1.33 \pm 0.25) \times 10^{-6}$
m_1 ($M_\odot$)	1.36 ± 0.20
$m_2 \sin i$ (M_{Jup})	14.2 ± 1.6
a (AU)	3.02 ± 0.15
i_{crit} (deg) (for $m_2 = 0.078\,M_\odot$)	10.4
$p(i \leqslant i_{\mathrm{crit}})$	1.6%

5. THE NATURE OF THE RADIAL VELOCITY VARIATIONS

5.1. Activity or Sub-stellar Companion?

Unfortunately, periodic RV variations can also be caused by stellar oscillations or stellar activity. For solar-like stars an oscillation period of 1634 days can be excluded. However, rotation periods and activity cycles may have the same periods as orbiting planets. Spots can produce RV signals that are quite similar to those of planets. It is thus not surprising that some planet detections had to be withdrawn, as it turned out that the RV variations were caused by spots. For example, Queloz et al. (2001) found RV variations with an amplitude $K = 83$ m s^{-1} in the young G0 dwarf HD 166435 that were, at first, interpreted as the signature of a 0.6 M_{Jup} planet in a 3.8-day orbit around the star. Later photometric and Ca II H and K spectro-photometric observations showed clearly that starspots producing a photometric amplitude of 0.05 mag were the cause of the observed RV variations. Further examples are HD 192263 and HD 83443. In the first case, Santos et al. (2000) and Vogt et al. (2000) claimed the detection of a 0.8 M_{Jup} planet with a period of 24 days, but Henry et al. (2002) subsequently showed that the star shows periodic photometric variations of the same period. Additionally, the Ca II H and K emission fluxes also varied with the same period. In the case of HD 83443, the

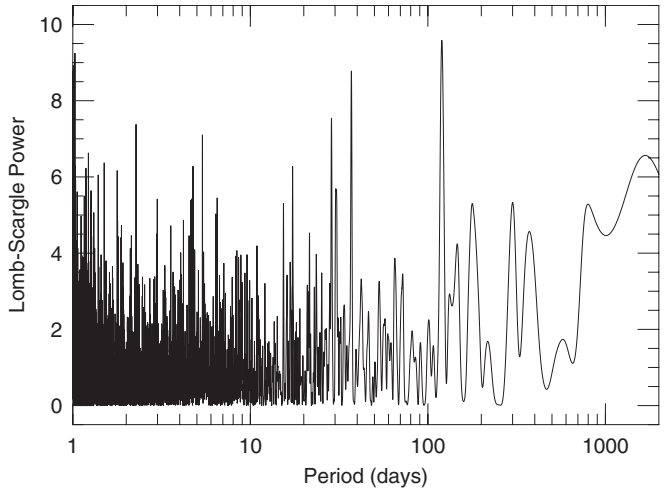

Figure 4. Lomb–Scargle periodogram of the RV residuals of HD 8673.

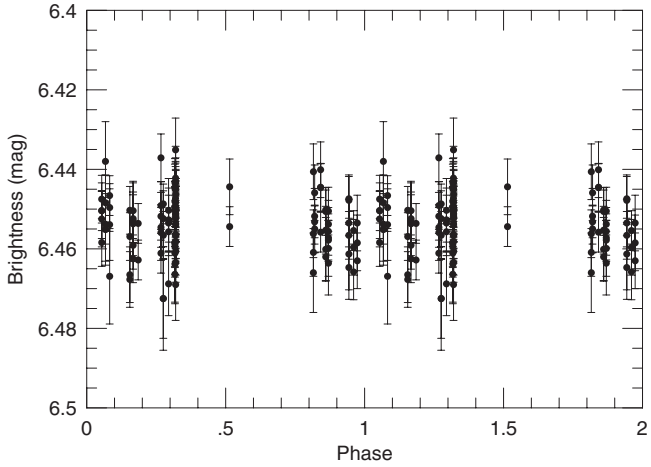

Figure 5. *Hipparcos* photometry of HD 8673 phased to the orbital period of 1634 days.

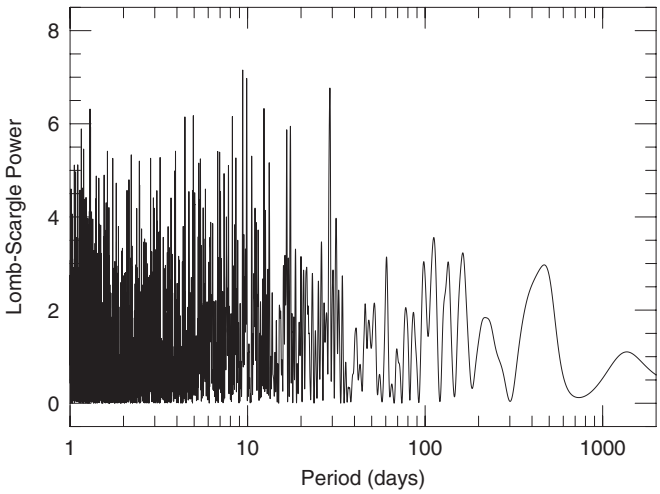

Figure 6. Lomb–Scargle periodogram of the *Hipparcos* photometry of HD 8673.

detection of two planets with periods of 2.985 and 29.8 days was claimed by Mayor et al. (2000). However, the inner planet was confirmed by additional RV measurements, but the outer planet was not (Butler et al. 2002; Mayor et al. 2004).

Using the stellar radius $R_\star = 1.54 \pm 0.06\,R_\odot$ and the measured projected rotational velocity $v \sin i = 28.4 \pm 0.8\,\mathrm{km\,s^{-1}}$ (see Table 1) results in a rotational period of $P_{\rm rot} \leqslant 2\pi\,R_\star/(v \sin i) = 2.74 \pm 0.13$ days. Thus, we can certainly rule out rotational modulation as the cause of the RV variations, but the RV period may still be due to an activity cycle.

The first test to exclude this possibility is to look for brightness variations. Although *Hipparcos* did not observe the star simultaneously with our RV measurements, we can use these data to investigate the typical spot coverage of the star. In total, 117 photometric measurements of HD 8673, which are displayed phase-folded to the orbital period in Figure 5, were carried out with the *Hipparcos* satellite. We searched the photometry data for periodicities, but did not find any significant variations as can be seen in the resulting Lomb–Scargle periodogram in Figure 6. The median brightness of the star in the *Hipparcos* photometric system is 6.4536 ± 0.0009 mag. The scatter of the photometric data is 0.0074 mag, which should be compared with the average error of 0.0066 mag. Using this value and the relation between filling-factor and the RV semi-amplitude as derived by Saar & Donahue (1997), we can estimate the spot-induced RV semi-amplitude to be about $62\,\mathrm{m\,s^{-1}}$ with an accuracy $\leqslant 20\%$. Compared to the derived RV amplitude $K = 288 \pm 16\,\mathrm{m\,s^{-1}}$, this is 4–5 times lower. We can also turn around the argument and use the equation from Paulson et al. (2002) to find that a spot would have to cover about 1.8% of the stellar surface, which means that the photometric variations would have to be 0.045 mag in order to explain the observed RV variations. Such brightness variations (almost a factor of 7 higher than the average error) should have been detected by the *Hipparcos* satellite.

The second test is to look for X-ray emission since an active star would have to be bright in X-rays and also in the radio regime. Figure 7 shows the *ROSAT* All Sky Survey image around HD 8673. There is in fact an X-ray source only 10 arcsec away from the position of HD 8673. The *ROSAT* All Sky Bright Source Catalog (1RXS; Voges et al. 1999) gives a brightness of 0.0625 ± 0.0165 counts $\mathrm{s^{-1}}$, which implies a ratio of the X-ray brightness to the optical flux $\log(f_{\rm X}/f_{\rm opt}) = -4.31$. How does this compare to other F7 V stars? In total, this ratio is given for 37 F7 V stars brighter than 7 mag in the *ROSAT* catalog. The values span a range from $\log(f_{\rm X}/f_{\rm opt}) = -5.01$ to -2.80, the average value is -3.96 ± 0.50 and the median -3.99. Hence, the X-ray brightness of HD 8673 is fairly typical for an F7 V star in the solar neighborhood. The star thus has a corona, but it is not more active than other F7 V stars.

As a next step, we took a spectrum in the wavelength region that covers the Ca II infrared lines. In active stars, these lines show an emission line core, like the Ca II H and K lines in the UV. Figure 8 shows the Ca II 8497.613 Å line for HD 8673 as well as for the active K0 V star HIP 114379E. In the case of HIP 114379E, an emission line core is clearly visible while this feature is not seen in the spectrum of HD 8673. Consequently, we conclude that HD 8673 is an inactive star.

The fourth test in order to find out whether the RVs are affected by stellar activity is to measure the asymmetry of spectral lines, i.e., the difference in velocity space between the lower and the upper part of the lines. Therefore, we used the unblended photospheric lines Fe I 6393.612 Å, Fe I 6400.009 Å, Ca I 6439.083 Å, Ni I 6643.638 Å, Fe I 6677.997 Å, Fe I 6750.164 Å, Ca I 6717.687 Å, and Ni I 6767.784 Å because this part of the spectrum is not contaminated by iodine lines. The average asymmetry of the lines is plotted against the measured

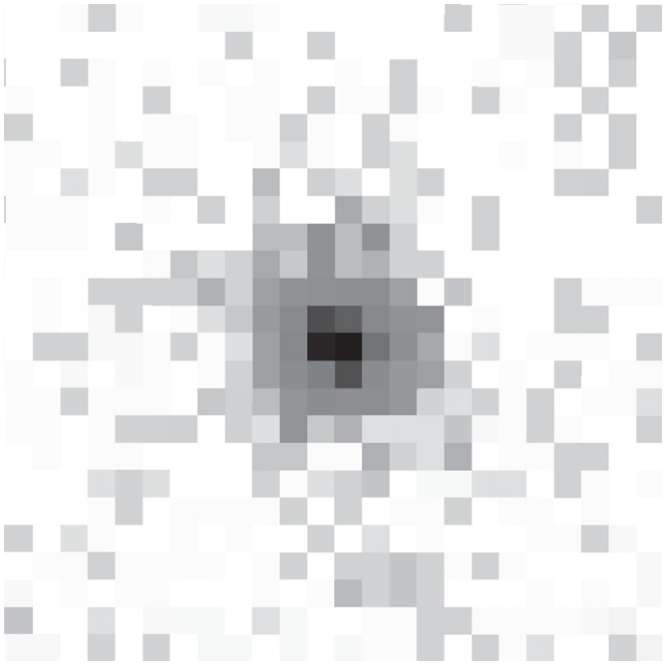

Figure 7. *ROSAT* All Sky Survey image showing the field around HD 8673. At the position of HD 8673, there is in fact a strong X-ray source.

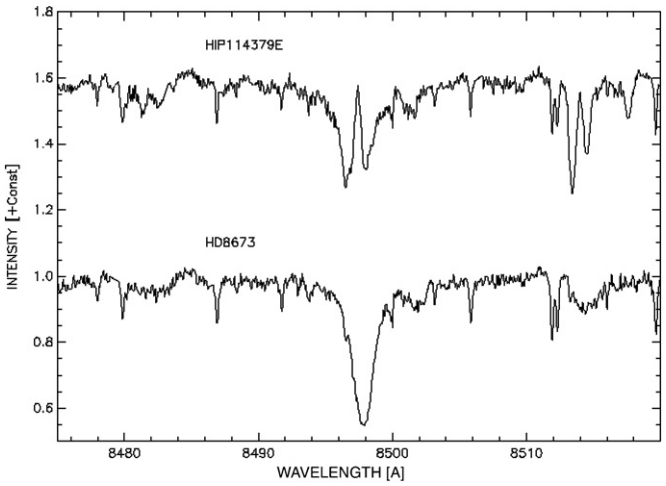

Figure 8. Spectrum of HD 8673 and the active K0 V star HIP 114379E. Typical for an active star is the emission core of the Ca II 8497.613 Å line. This component is not seen in the spectrum of HD 8673; we thus consider it as inactive.

RV in Figure 9. Given the small number of lines used in this analysis, the errors of the bisector asymmetry are much worse than those of the RV measurements. Nevertheless, there is no correlation between the two quantities. A periodogram analysis of the bisector asymmetry data showing no significant features in the corresponding Lomb–Scargle periodogram (Figure 10) was also carried out.

All four tests thus speak against the activity cycle hypothesis and favor the companion hypothesis.

5.2. Is it a Planet or a Binary Viewed Almost Face-on?

One principal problem of the RV method is that only $m_2 \sin i$ and not the true mass of the companion can be determined. Using the mass limit of 0.078 $M_\odot$ between brown dwarfs and stars, the critical orbital inclination would be $i_{\rm crit} = 10\overset{\circ}{.}4$. Accordingly, a companion having an inclination $i < i_{\rm crit}$ would be a binary

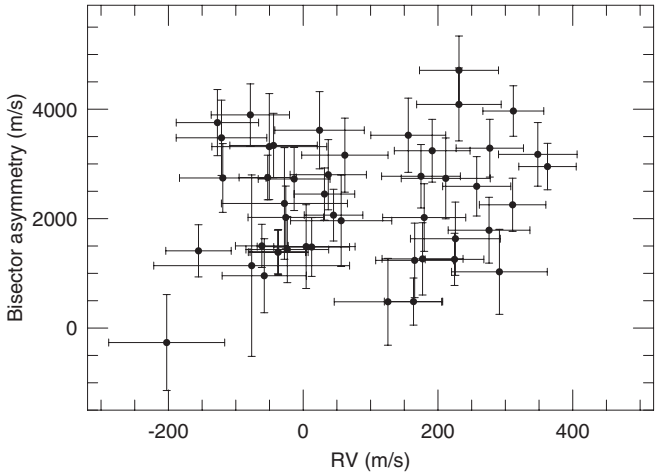

Figure 9. Asymmetry of the line bisector measured from eight spectral lines plotted against the RV. The absence of a correlation indicates that the RV variations are not caused by stellar activity.

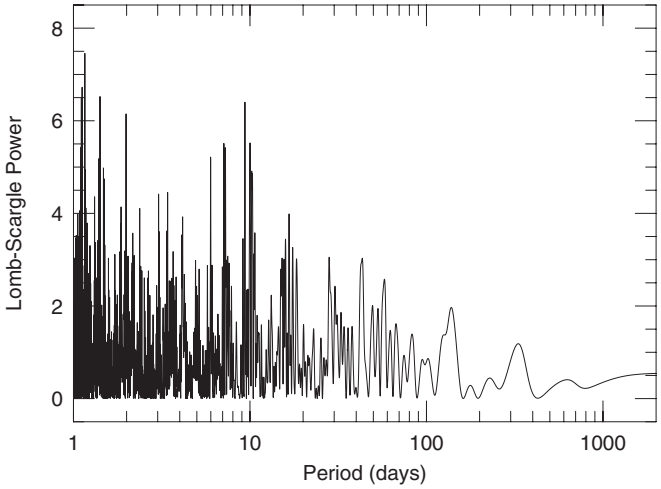

Figure 10. Lomb–Scargle periodogram of the measured bisector asymmetry of HD 8673.

and not a sub-stellar object. Assuming a random orientation of the orbit, the probability that i is smaller than $i_{\rm crit}$ is given by $p(i < i_{\rm crit}) = 1 - \cos i_{\rm crit}$. The probability for the companion to have an inclination $< 10\overset{\circ}{.}4$ is in fact only 1.6%, making it very unlikely that the companion is a star (see also Table 3). One way to securely exclude this possibility is through astrometric measurements. Using the distance and mass of the star in addition to the derived orbital parameters of the companion, the projected motion of the star on the plane of the sky would be an ellipse with an angular semi-major axis $\alpha \geqslant 4.3$ mas if the mass of the companion is stellar ($m_2 \geqslant 0.078\,M_\odot$). The *Hipparcos* astrometric observations of HD 8673 were made between epochs 1989.94 and 1993.06, hence covering about 70% of the orbital period of the companion. In Figure 11, we show the predicted astrometric orbits of the primary due to its companion for different inclination angles. Proper and parallactic motion are not taken into account. The positions on these orbits according to the times of the *Hipparcos* measurements are marked by the points. The first measurements were done around the periastron (1989.98), later measurements around the co-vertex of the ellipse (1990.58) and around the apastron (1992.21), which means that the orbital motion from periastron to apastron caused by the companion (corresponding to a linear projected distance

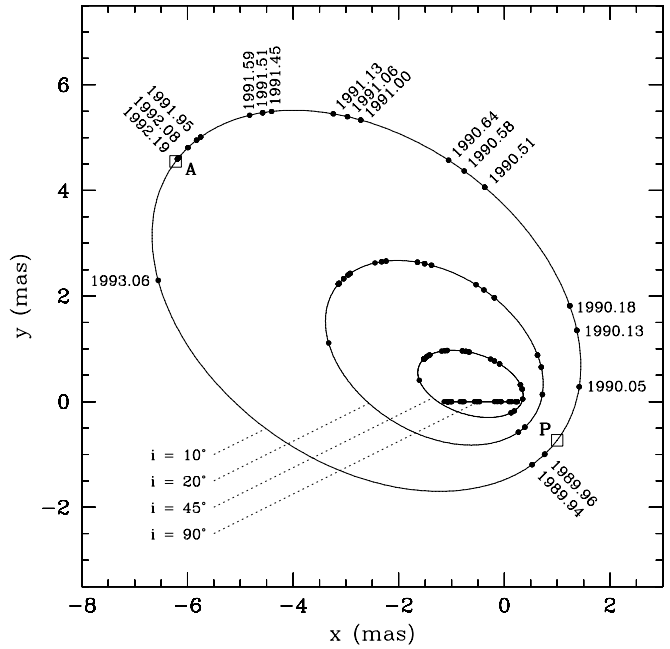

Figure 11. Predicted astrometric orbits of HD 8673 due to its companion (without proper and parallactic motion) for inclination angles $i = 10°, 20°, 45°$, and 90° (solid lines). The corresponding secondary masses are 0.08 $M_{\odot}$, 42.2, 20.2, and 14.2 $M_{\rm Jup}$, respectively. The points represent the positions on these orbits according to the times when the *Hipparcos* astrometric measurements were made. The open squares mark the location of periastron (P) and apastron (A) passage.

of $\geqslant$8.6 mas for $i \leqslant 10\overset{\circ}{.}4$) would have been recorded. This signature would have been detected by the *Hipparcos* mission.

Direct imaging techniques using coronagraphy, nulling interferometry, or pupil modification could also be applied in order to detect faint light sources in the close stellar environment and thus place constraints on the orbital inclination. Several coronagraphic concepts have been proposed, which uses advanced focal plane masks to eliminate the light of the central star (e.g., Guyon et al. 1999; Rouan et al. 2000; Kuchner & Traub 2002). Since the classical two-telescope interferometer (Bracewell 1978) can extinguish an on-axis point source almost perfectly, it remains limited by residual light from off-axis rays of resolved stars. Therefore, some nulling interferometry configurations with more than two telescopes were studied (e.g., Angel & Woolf 1997; Mennesson & Mariotti 1997). In contrast, the pupil modification method can only reduce the brightness of the diffraction lobes via shaped or apodized pupils (e.g., Nisenson & Papaliolios 2001; Kasdin et al. 2003). The combination of the nulling interferometer with a nulling coronagraph (Guyon & Roddier 2002) or with a modified pupil (Nishikawa et al. 2005) was also investigated. More recently, a new interferometric technique called "phase closure nulling" has been introduced by Chelli et al. (2009). Here, the influence of a companion is determined by measuring the phase closure of the system near the visibility nulls of the primary, where the phase closure signature of the secondary is at its maximum and larger than any systematic error. The potential of this method was demonstrated by analyzing AMBER/VLTI observations of the single-lined spectroscopic binary HD 59717 (Duvert et al. 2010).

The measured projected rotational velocity of $v \sin i = 28.4\,{\rm km\,s^{-1}}$ for HD 8673 can also be used to argue against seeing the orbit pole-on provided that orbital and stellar spin axes are aligned. For inclination angles $i \leqslant 10\overset{\circ}{.}4$, i.e., $\sin i \leqslant 0.18$, one obtains $v \gtrsim 158\,{\rm km\,s^{-1}}$ and $P_{\rm rot} \lesssim 0.5$ days. Nordström et al. (1997) measured rotational velocities for 595 early F-type dwarfs including 530 single-lined and 65 double-lined stars. For the single-lined stars, they used three different effective temperatures as template spectrum parameter, namely 6500, 6750, and 7000 K. The value of 6500 K gives the closest match to HD 8673. Considering only the 40 single-lined stars with this value yields a mean (median) $v \sin i$ of 36.6 (33.8) ${\rm km\,s^{-1}}$. The data set ranges from 7.6 to 95.0 ${\rm km\,s^{-1}}$. Obviously, the lowest (highest) values correspond to stars with a spin axis that is nearly seen pole-on (edge-on). That implies that the maximum value of $v \sin i$ represents roughly the maximum value of v which makes it extremely unlikely for a mid- or late-F-type dwarf to rotate more rapidly than $\approx$100 ${\rm km\,s^{-1}}$.

We therefore can definitely exclude HD 8673 as a binary star viewed face-on. While the companion could still be a supermassive planet, it is most likely a low-mass brown dwarf.

6. DISCUSSION AND CONCLUSION

We have discovered significant variations in our RV measurements for the F7 V star HD 8673 with a period of 1634 ± 17 days. Since HD 8673 is not more active than other F7 V stars in the solar neighborhood (i.e., similar X-ray emission, no emission line core of the Ca II infrared lines) and because of the absence of any correlation between line asymmetry and RV, we interpret these variations as the signature of an orbiting companion. Additionally, the *Hipparcos* data as well as the measured $v \sin i$ allow us to exclude a binary star viewed face-on. We thus conclude that HD 8673 is orbited by a very massive planet or low-mass brown dwarf, whose properties make it indeed an object of special interest. With a minimum mass of $14.2 \pm 1.6\,M_{\rm Jup}$—slightly above the deuterium burning limit of 13 $M_{\rm Jup}$—and a very high eccentricity of $e = 0.723 \pm 0.016$, it is among the 15 exoplanet objects with the highest values in minimum mass and eccentricity known so far.

Since planet formation occurs in a circumstellar disk, one would expect that planetary orbits would be nearly circular. In order to explain the high eccentricities of extrasolar planets, several eccentricity excitation mechanisms have been established: interactions with the protoplanetary gas disk (Goldreich & Sari 2003), gravitational planet–planet interactions in multi-planet systems (Marzari & Weidenschilling 2002; Chatterjee et al. 2008; Jurić & Tremaine 2008), or external perturbations due to a stellar companion in a binary (Mazeh et al. 1997) or a nearby passing star in a cluster (Zakamska & Tremaine 2004; Malmberg et al. 2007).

An interesting question in this context is whether planets of different masses show differences in their eccentricity distribution. Marcy et al. (2005) found no strong correlation between planetary mass and eccentricity. However, they claimed that higher mass planets ($m_2 \sin i > 5\,M_{\rm Jup}$) exhibit systematically higher eccentricities than planets of lower mass. A similar study was carried out before by Udry et al. (2002). Searching for differences of the distributions of orbital and stellar-host properties of two planetary mass subclasses (limit at 4 $M_{\rm Jup}$), they found a high peak of "light" planets at small eccentricities representing the short-period, close-in planets that were probably circularized. They also stated that excluding all planets having periods less than 50 days, the mentioned peak which was mainly responsible for the difference observed in the cumulative functions disappeared. Compared to the year 2002, the number of discovered exoplanets has increased by a factor of ~2.5, so that an improved statistic can be done.

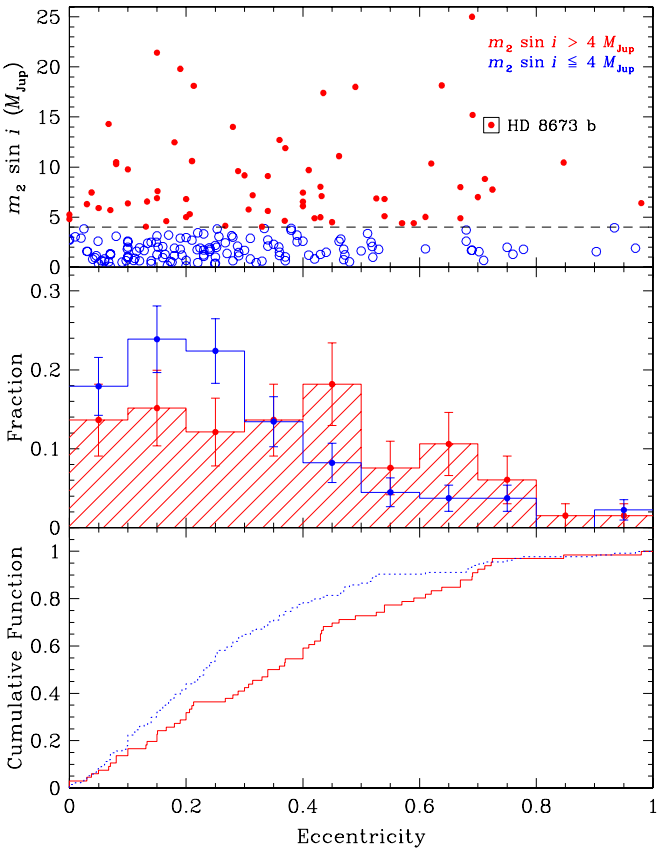

Figure 12. Comparison of the eccentricity distribution of extrasolar planets with different masses: m_2 sin $i \leqslant 4\,M_{\rm Jup}$ (blue color, open circles, open histogram, dotted line) and m_2 sin $i > 4\,M_{\rm Jup}$ (red color, filled circles, shaded histogram, solid line). The open square in the upper panel represents the companion of HD 8673.

In Figure 12 (upper panel), we plot m_2 sin i versus eccentricity for all extrasolar planets listed in the *Extrasolar Planets Encyclopedia*[2] as of 2009 October. Therefore, we consider only planets with periods larger than 100 days as planets in shorter and tighter orbits might be influenced by tidal circularization. In addition, we divided the sample into two mass subclasses, setting the limit at 4 $M_{\rm Jup}$. The middle and lower panels of Figure 12 show the histograms and cumulative functions of the subclasses. The two distributions are different in two parts: first, the distribution of "light" planets features a significant peak at eccentricities $0.1 \leqslant e < 0.3$, where the fraction is roughly a factor of 2 higher than the fraction of "massive" planets. Such a peak is not seen for the "massive" planet subclass; the trend is rather flat up to eccentricities of ∼0.4. Second, in the range $0.4 \leqslant e < 0.7$, the rate of "massive" planets is larger (again by about a factor of 2) than those of "light" planets. The distribution of "massive" planets may have a small peak at $0.4 \leqslant e < 0.5$, although this is not significant. In all other regions the two distributions are not distinguishable. From the cumulative functions one can easily read off the median eccentricities for the "light" and "massive" planet subclass, namely 0.23 and 0.35, respectively.

Therefore, given the current known sample of exoplanets, there appears to be a clear trend for massive planets to have higher orbital eccentricities.

We are grateful to the user support group of the Alfred-Jensch telescope: B. Fuhrmann, J. Haupt, C. Högner, M. Kehr, U. Laux, F. Ludwig, M. Pluto, J. Schiller, and J. Winkler. A.P.H. and M.H. acknowledge the support of grant HA 3279/3-2 from the Deutsche Forschungsgemeinschaft (DFG). We thank the anonymous referee for helpful comments that improved this paper. This research has made use of the SIMBAD database, operated at CDS, Strasbourg, France.

Facilities: TLS

[2] http://exoplanet.eu

REFERENCES

Angel, J. R. P., & Woolf, N. J. 1997, ApJ, 475, 373
Bonfils, X., et al. 2005, A&A, 443, L15
Bracewell, R. N. 1978, Nature, 274, 780
Butler, R. P., Johnson, J. A., Marcy, G. W., Wright, J. T., Vogt, S. S., & Fischer, D. A. 2006, PASP, 118, 1685
Butler, R. P., Marcy, G. W., Williams, E., McCarthy, C., Dosanjh, P., & Vogt, S. S. 1996, PASP, 108, 500
Butler, R. P., et al. 2002, ApJ, 578, 565
Cayrel de Strobel, G., Soubiran, C., & Ralite, N. 2001, A&A, 373, 159
Chatterjee, S., Ford, E. B., Matsumura, S., & Rasio, F. A. 2008, ApJ, 686, 580
Chelli, A., Duvert, G., Malbet, F., & Kern, P. 2009, A&A, 498, 321
Cumming, A. 2004, MNRAS, 354, 1165
Cumming, A., Butler, R. P., Marcy, G. W., Vogt, S. S., Wright, J. T., & Fischer, D. A. 2008, PASP, 120, 531
Döllinger, M. P., Hatzes, A. P., Pasquini, L., Guenther, E. W., Hartmann, M., Girardi, L., & Esposito, M. 2007, A&A, 472, 649
Duvert, G., Chelli, A., Malbet, F., & Kern, P. 2010, A&A, 509, A66
Endl, M., Cochran, W. D., Kürster, M., Paulson, D. B., Wittenmyer, R. A., MacQueen, P. J., & Tull, R. G. 2006, ApJ, 649, 436
ESA 1997, The *Hipparcos* and *Tycho* Catalogues (ESA SP-1200; Noordwijk: ESA)
Fuhrmann, K. 2008, MNRAS, 384, 173
Galland, F., Lagrange, A.-M., Udry, S., Chelli, A., Pepe, F., Queloz, D., Beuzit, J.-L., & Mayor, M. 2005, A&A, 443, 337
Goldreich, P., & Sari, R. 2003, ApJ, 585, 1024
Guenther, E. W., Hartmann, M., Esposito, M., Hatzes, A. P., Cusano, F., & Gandolfi, D. 2009, A&A, 507, 1659
Guyon, O., & Roddier, F. 2002, A&A, 391, 379
Guyon, O., et al. 1999, PASP, 111, 1321
Hatzes, A. P., et al. 2006, A&A, 457, 335
Henry, G. W., Donahue, R. A., & Baliunas, S. L. 2002, ApJ, 577, L111
Ibukiyama, A., & Arimoto, N. 2002, A&A, 394, 927
Jefferys, W. H., Fitzpatrick, M. J., & McArthur, B. E. 1988, Celest. Mech., 41, 39
Johnson, J. A., Butler, R. P., Marcy, G. W., Fischer, D. A., Vogt, S. S., Wright, J. T., & Peek, K. M. G. 2007a, ApJ, 670, 833
Johnson, J. A., Marcy, G. W., Fischer, D. A., Henry, G. W., Wright, J. T., Isaacson, H., & McCarthy, C. 2006, ApJ, 652, 1724
Johnson, J. A., et al. 2007b, ApJ, 665, 785
Jurić, M., & Tremaine, S. 2008, ApJ, 686, 603
Kasdin, N. J., Vanderbei, R. J., Spergel, D. N., & Littman, M. G. 2003, ApJ, 582, 1147
Kennedy, G. M., & Kenyon, S. J. 2008, ApJ, 673, 502
Kornet, K., Wolf, S., & Różyczka, M. 2006, A&A, 458, 661
Kuchner, M. J., & Traub, W. A. 2002, ApJ, 570, 900
Kürster, M., Schmitt, J. H. M. M., Cutispoto, G., & Dennerl, K. 1997, A&A, 320, 831
Lomb, N. R. 1976, Ap&SS, 39, 447
Lovis, C., & Mayor, M. 2007, A&A, 472, 657
Malmberg, D., de Angeli, F., Davies, M. B., Church, R. P., Mackey, D., & Wilkinson, M. I. 2007, MNRAS, 378, 1207
Marcy, G., Butler, R. P., Fischer, D., Vogt, S., Wright, J. T., Tinney, C. G., & Jones, H. R. A. 2005, Prog. Theor. Phys. Suppl., 158, 24
Marzari, F., & Weidenschilling, S. J. 2002, Icarus, 156, 570
Mayor, M., Naef, D., Pepe, F., Queloz, D., Santos, N. C., Udry, S., & Burnet, M. 2000, in IAU Symp. 202, Planetary Systems in the Universe: Observation, Formation and Evolution, ed. A. Penny et al. (San Francisco, CA: ASP)
Mayor, M., Udry, S., Naef, D., Pepe, F., Queloz, D., Santos, N. C., & Burnet, M. 2004, A&A, 415, 391
Mazeh, T., Krymolowski, Y., & Rosenfeld, G. 1997, ApJ, 477, L103
Mennesson, B., & Mariotti, J. M. 1997, Icarus, 128, 202
Niedzielski, A., et al. 2007, ApJ, 669, 1354
Nisenson, P., & Papaliolios, C. 2001, ApJ, 548, L201
Nishikawa, J., Kotani, T., Murakami, N., Baba, N., Itoh, Y., & Tamura, M. 2005, A&A, 435, 379

Nordström, B., Stefanik, R. P., Latham, D. W., & Andersen, J. 1997, A&AS, 126, 21
Nordström, B., et al. 2004, A&A, 418, 989
Paulson, D. B., Saar, S. H., Cochran, W. D., & Hatzes, A. P. 2002, AJ, 124, 572
Perryman, M. A. C., et al. 1997, A&A, 323, L49
Queloz, D., et al. 2001, A&A, 379, 279
Rouan, D., Riaud, P., Boccaletti, A., Clénet, Y., & Labeyrie, A. 2000, PASP, 112, 1479
Saar, S. H., & Donahue, R. A. 1997, ApJ, 485, 319
Santos, N. C., Mayor, M., Naef, D., Pepe, F., Queloz, D., Udry, S., Burnet, M., & Revaz, Y. 2000, A&A, 356, 599
Sato, B., et al. 2007, ApJ, 661, 527
Scargle, J. D. 1982, ApJ, 263, 835
Takeda, G., Ford, E. B., Sills, A., Rasio, F. A., Fischer, D. A., & Valenti, J. A. 2007, ApJS, 168, 297
Udry, S., Mayor, M., Naef, D., Pepe, F., Queloz, D., Santos, N. C., & Burnet, M. 2002, A&A, 390, 267
Valenti, J. A., Butler, R. P., & Marcy, G. W. 1995, PASP, 107, 966
Valenti, J. A., & Fischer, D. A. 2005, ApJS, 159, 141
Voges, W., et al. 1999, A&A, 349, 389
Vogt, S. S., Marcy, G. W., Butler, R. P., & Apps, K. 2000, ApJ, 536, 902
Zakamska, N. L., & Tremaine, S. 2004, AJ, 128, 869
Zechmeister, M., & Kürster, M. 2009, A&A, 496, 577